Available online at www.sciencedirect.com
SCIENCE DIRECT
Catalysis Today 114 (2006) 388–396
CATALYSIS TODAY
www.elsevier.com/locate/cattod

Synthesis of ZSM-5/SAPO-11 composite and its application in FCC gasoline hydro-upgrading catalyst

Yu Fan [a,b], Duo Lei [b], Gang Shi [b], Xiaojun Bao [a,b,*]

[a] State Key Laboratory of Heavy Oil Processing, China University of Petroleum, Beijing 102249, PR China
[b] The Key Laboratory of Catalysis, China National Petroleum Co., China University of Petroleum, Beijing 102249, PR China

Available online 3 April 2006

Abstract

This article describes the synthesis, characterization and application of a novel aluminosilicate/silicoaluminophosphate composite zeolite ZSM-5/SAPO-11. The composite was synthesized by the in situ overgrowth of SAPO-11 on ZSM-5 and was characterized by means of X-ray diffraction (XRD), scanning electron microscopy (SEM), Fourier transformed infrared (FT-IR) spectrometry, N_2 adsorption and infrared spectroscopy of adsorbed pyridine. The results were compared with those of the mechanical mixture composed of individual ZSM-5 and SAPO-11. In the mechanical mixture, the ZSM-5 phase was morphologically separate from the SAPO-11 phase, while the ZSM-5/SAPO-11 composite existed in a form of a core-shell structure, with the ZSM-5 phase as the core and the SAPO-11 phase as the shell. Compared with the mechanical mixture, the composite had more mesopores and moderate acidity distribution, which could accelerate the diffusion of substances and enhance the synergetic effect between Brönsted and Lewis acids. The comparison of the catalytic performances of the mechanical mixture and the composite-based Ni–Mo catalysts for FCC gasoline hydro-upgrading showed that, due to the above advantages of the composite, the corresponding catalyst yielded improved gasoline research octane number, high liquid yield, good desulfurization activity and lower coke amount and thus could be considered as a potential catalyst system for hydro-upgrading FCC gasoline.

Keywords: ZSM-5/SAPO-11 composite; Synthesis; Characterization; FCC gasoline hydro-upgrading

1. Introduction

Air pollution in urban regions caused by exhaust emissions from gasoline-powered motor vehicles has become a serious issue in both developed and developing countries due to the high content of sulfur compounds and olefins in most gasoline. In air, unburned olefins can easily react with NO_x to form photo-chemical smog, and sulfur compounds can degrade the effectiveness of automobile catalytic converters for NO_x, CO, and hydrocarbon emissions control by poisoning three-way catalysts. Thus, most of the countries over the world have tightened their regulations on gasoline compositions, especially on the contents of sulfur compounds and olefins. It has been reported that more than 90% of sulfur compounds and about 90% of olefins in typical refinery gasoline pools come from FCC gasoline [1], so this stream is obviously a focal point in producing clean gasoline. In China, approximately 80% of the gasoline pool comes from FCC gasoline, resulting in higher sulfur and olefin contents in the commercial gasoline. Various measures (such as optimization of the FCC process, use of new FCC catalysts [2], or selective hydrogenation [3,4]) have been taken, but none of them enables satisfactory sulfur and olefin control without loss in the gasoline research octane number (RON). Therefore, it is still a great challenge for the refineries in China to produce the clean gasoline that meets the more stringent specification of clean fuels.

In order to reduce the contents of sulfur compounds and olefins of FCC gasoline as well as preserve its RON, researchers have proposed various hydro-upgrading processes that combine hydrodesulfurization (HDS) with hydrocracking and hydro-isomerization [5–7], but most of them involve a high operating cost because of lower gasoline yield. In previous papers [8–10], we found that reducing the olefin content in FCC gasoline by only hydroisomerization was unable to preserve gasoline RON. Because the arene content in FCC gasoline produced in China is usually in the range of 12–18 vol.%, much lower than 35 vol.%

* Corresponding author. Fax: +86 10 8973 4979.
E-mail address: baoxj@cup.edu.cn (X. Bao).

0920-5861/$ – see front matter © 2006 Elsevier B.V. All rights reserved.
doi:10.1016/j.cattod.2006.02.050

as regulated by Category 3 Unleaded Gasoline of the World-Wide Fuel Charter, there is some leeway to preserve gasoline RON by converting olefins (especially C_5–C_7 olefins) in FCC gasoline into *i*-paraffins and arenes that have higher RON. Thus, from the point of view of olefin and sulfur content reduction as well as gasoline RON preservation, a novel catalyst system with balanced desulfurization, olefin hydroisomerization and olefin aromatization abilities need to be developed. Intuitively, it is expected that this kind of catalyst system can be obtained by combining or compositing different zeolites with desired properties. It has been widely recognized that zeolite ZSM-5 has excellent activity for both HDS [11,12] and light alkane and alkene aromatization [13–15]. Moreover, silicoaluminophosphate zeolite SAPO-11 has been widely applied to the isomerization of C_4–C_7 hydrocarbons for producing gasoline with high RON [16–19] and to the dewaxing process for making high quality diesel and lube oil basestocks via isomerization of long-chain alkanes [20,21] due to its superior hydroisomerization activity. Naturally, it is reasonable to conceive that a catalyst system based on a ZSM-5/SAPO-11 composite with suitable composition should provide a balanced desulfurization, hydroisomerization and aromatization performance and thereby benefit the upgrading of FCC gasoline. While reports on the synthesis and applications of aluminosilicate/aluminosilicate composite zeolites are abundant in literatures, as extensively reviewed by Smirniotis and Davydov [22], only limited information is available on the preparation and application of aluminosilicate/silicoaluminophosphate composite zeolites [23,24]. In addition, most of the composite zeolites reported in the literatures consisted of two or more individual zeolites mixed mechanically; few of them were made by synthesis. The mechanical mixing may inhibit the intimate contacts of different zeolites and thereby downgrade their synergism. For this purpose, a series of aluminosilicate/silicoaluminophosphate ZSM-5/SAPO-11 composites were synthesized by a two-step crystallization method in the present investigation. They were characterized by means of X-ray diffraction (XRD), scanning electron microscopy (SEM), N_2 adsorption, Fourier transformed infrared spectroscopy (FT-IR) and infrared spectroscopy of adsorbed pyridine. In addition to this, composite-supported Ni–Mo catalysts were made and their catalytic performance for upgrading FCC gasoline was assessed.

2. Experimental

2.1. Synthesis of SAPO-11 and ZSM-5

SAPO-11 was synthesized according to the method reported by Lok et al. [25]. The detailed procedure was described elsewhere [9].

ZSM-5 was synthesized as follows: firstly, aluminum sulfate (Beijing Chemical Co., PR China) was dissolved in distilled water, followed by the addition of sulfuric acid (98 wt.%; Beijing Chemical Co., PR China) to form solution A; secondly, tetraethylammonium hydroxide (TEAOH) (20 wt.%; Beijing Chemical Co., PR China), distilled water and sodium silicate (26.3 wt.% SiO_2, 8.2 wt.% Na_2O; Beijing Aviation Materials Institute, PR China) were mixed in proper proportions to form solution B; thirdly, solution A was slowly added to solution B under agitation. The resulting mixture with the molar composition of 9.7 Na_2O:1 Al_2O_3:40 SiO_2:10 $(TEA)_2O$:1800 H_2O was further stirred vigorously for 1 h to get a homogenous gel. Fourthly, the gel was then moved to a 150 ml stainless steel autoclave and heated at 448 K for 72 h; finally, the resulting solid was filtrated, washed with deionized water, dried overnight at 383 K, and calcined in air at 823 K for 4 h to remove the organic template.

2.2. Synthesis of ZSM-5/SAPO-11 composite

The synthesis of ZSM-5/SAPO-11 composite is schematically depicted in Fig. 1.

In the first step, zeolite ZSM-5 was synthesized by the method mentioned above, except that its crystallization time was shortened to 48 h and post-treatments (such as filtration, washing, drying and calcination) were omitted.

In the second step, ZSM-5/SAPO-11 composite was synthesized by the following procedure: firstly, a diluted solution of phosphoric acid (85 wt.%; Beijing Jinxing Chemical Plant, PR China) in distilled water was prepared; secondly, pseudoboehmite (73 wt.% Al_2O_3; Tianjin Hengmeilin Chemical Co., PR China) and silica sol (25 wt.% SiO_2; Beijing Changhong Chemical Plant, PR China) were slowly added to the phosphoric acid solution and the resulting mixture was vigorously stirred for 2.5 h; thirdly, the uniform mixture obtained and di-*n*-propylamine (DPA) (99 wt.%; Beijing Jinxing Chemical Plant, PR China) were subsequently added drop by drop into the above crystallization product of ZSM-5 to allow at least 2 h stirring before they were completely added. The molar composition of the resulting homogenous gel was 1 DPA:1 Al_2O_3:1 P_2O_5:0.3 SiO_2:50 H_2O. Fourthly, the gel was moved into stainless steel autoclaves (150 ml) and heated at 458 K for 24 h. Fifthly, the solid product recovered by centrifugation was washed with deionized water and dried at 383 K for 12 h. Finally, to remove amine the solid product was calcined at 823 K for 8 h at a heating rate of 2 K/min, with two stops at 553 and 663 K for 1 h each, before the final calcination temperature was reached.

2.3. Catalyst preparation

The bifunctional catalysts investigated in this work are composed of H-form zeolites as the acid part, Ni–Mo as the metal part, and a binder (pseudoboehmite). The catalyst preparation procedure consists of three main steps: preparation of H-type zeolites, incorporation of metallic function, and activation of the metal part. Firstly, in order to obtain H-form zeolites, ion exchange was carried out three times (each time for 3 h) with 1 M NH_4NO_3 solution at 353 K, followed by calcination in air at 823 K for 4 h; then, the supported catalysts were prepared by impregnating H-form zeolites with $(NH_4)_6Mo_7O_{24}$ (Beijing Chemical Co., PR China) and $Ni(NO_3)_2$ (Beijing Chemical Co., PR China) using the fractional step method. Finally, the impregnated solids were extruded using pseudoboehmite as binder and then calcined at 773 K for 4 h.

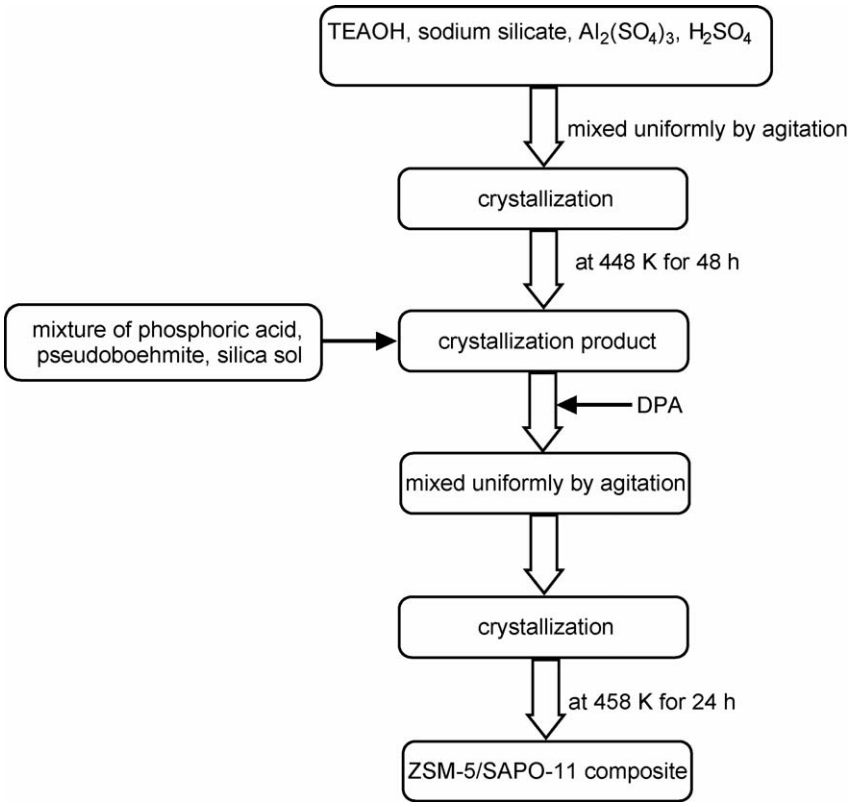

Fig. 1. Schematic for synthesizing ZSM-5/SAPO-11 composite.

2.4. Characterization

The phase structures of the calcined samples were characterized by XRD (Shimadzu 6000, Japan) using Cu Kα radiation. The instrument was operated at 40 kV and 30 mA with 2θ scanning speed at 4°/min; diffraction lines of 2θ between 5° and 35° were obtained. The mass fraction of SAPO-11 in ZSM-5/SAPO-11 composites was calculated from the integral intensity of the diffraction peak at $2\theta = 21.1°$ where there was no diffraction peak of ZSM-5. Similarly, the mass fraction of ZSM-5 in the composites was calculated at $2\theta = 7.8°$. The working curves were obtained by plotting the intensity of the diffraction peak at $2\theta = 21.1°$ versus the mass fraction of SAPO-11 and the intensity of the diffraction peak at $2\theta = 7.8°$ versus the mass fraction of ZSM-5, respectively, by measuring a series of mechanical mixtures prepared with known mass fractions of SAPO-11 and ZSM-5 in them.

The crystal size, the morphology and the elemental composition of the samples were determined by SEM (435VP, LEO, UK) equipped with an energy-dispersive X-ray spectrometer (EDS, Link-ISIS-300, Oxford, UK).

N_2 adsorption and desorption isotherms were obtained at 77 K using a volumetric adsorption apparatus (ASAP 2405N, Micromeritics, USA). The pore structures were estimated according to the Brunauer–Emmett–Teller (BET) method and the static volumetry. The samples were degassed at 573 K for 24 h under vacuum prior to the analysis.

The IR spectra were measured on a MAGNA-IR 560 FTIR instrument (Nicolet Co., USA) with a resolution of 1 cm^{-1}. The samples, each 15 mg, were extruded into the self-supported circular wafers 12 mm in diameter. The wafers were evacuated in situ in an IR cell at 623 K for 4 h, and after the temperature was decreased to room temperature, IR spectra were recorded. Subsequently, the samples were dehydrated at 773 K for 5 h under a vacuum of 1.33×10^{-3} Pa, followed by the adsorption of purified pyridine vapor at room temperature for 20 min. Finally, the system was evacuated at different temperatures and pyridine-adsorbed IR spectra were recorded.

2.5. Catalytic performance assessment

The catalytic performance assessment experiments were carried out in a flowing-type apparatus designed for continuous operation. This apparatus consists of a gas-feeding system controlled by a mass flowmeter and a syringe pump liquid feeding system. The reactor, with an internal diameter of 10 mm, was filled with the catalyst sample (ca. 6 g). There were three heating zones in the reactor, with the top one as the preheater. The temperature of each zone was independently controlled within ±1 K by thermostats. The temperature of the catalytic bed was measured by a thermocouple placed inside the reactor and was kept constant (±1 K). The reaction products were analyzed by an Agilent 1790 gas chromatograph to which a flame ionization detector and a HP-PONA capillary column (50 m × 0.2 mm) were attached. The coke deposited on the catalysts after the reaction was quantified by an automatic carbon analyzer (HV-4B, Wuxi Analysis Instruments Inc., PR China).

Table 1
Properties of FCC gasoline

Density (20 °C, g cm^{-3})	S (μg g^{-1})	Benzene (vol.%)	RON	Lumped composition (vol.%)				
				n-Paraffins	*i*-Paraffins	Olefins	Naphthenes	Arenes
0.714	300	0.68	91.7	6.3	28.3	41.1	7.0	17.4

In all runs, the catalysts to be tested were brought to the identical reaction conditions. The presulfurization of the catalysts was firstly carried out at 503, 563 and 593 K for 6 h, respectively, by flowing a stream containing 3 wt.% CS_2 in octane over the catalysts; then, pure hydrogen gas and FCC gasoline were fed into the reactor at a predetermined flow rate after the temperature was increased to the reaction temperature; finally, the reaction was carried out under the conditions of temperature 643 K, FCC gasoline liquid hourly space velocity (LHSV) 2 h^{-1}, total pressure 2.0 MPa, and volumetric ratio of H_2 to oil 200. The properties of FCC gasoline used are listed in Table 1.

3. Results and discussion

3.1. XRD

The XRD patterns of the samples are shown in Fig. 2. The typical characteristic peak at $2\theta = 7.8^\circ$ attributed to ZSM-5 and that at $2\theta = 21.1^\circ$ attributed to SAPO-11 can be clearly visualized in the diffraction pattern of the ZSM-5/SAPO-11 composite, despite the fact that some characteristic peaks attributed to individual ZSM-5 and SAPO-11 phases overlap with each other, demonstrating that both ZSM-5 and SAPO-11 phases are present in the composite obtained.

3.2. SEM

The SEM images of the samples are presented in Fig. 3. As shown in Figs. 3a and b, the single SAPO-11 phase is present in the form of pseudo-spherical aggregates of the size ranging from 7 to 8 μm consisting of uniform cubic plate monocrystals

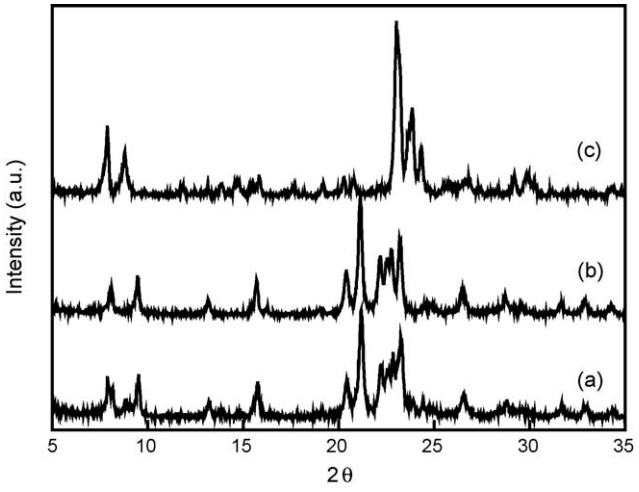

Fig. 2. XRD patterns of (a) the composite, (b) SAPO-11 and (c) ZSM-5.

ca. 0.5 μm in size (Fig. 3a), and the ZSM-5 phase alone is present in the form of spherical aggregates of the size ranging from 3 to 5 μm consisting of nonuniform columnar monocrystals ca. 1 μm long (Fig. 3b). For the mechanical mixture of ZSM-5 and SAPO-11, Fig. 3c clearly shows that the large pseudo-spherical particles assigned to SAPO-11 are separate from the small spherical ones assigned to ZSM-5. For the SAPO-11/ZSM-5 composite obtained by the overgrowth of SAPO-11 on ZSM-5, however, the ZSM-5 phase in the composite is covered by a film of SAPO-11 (Fig. 3d and e), showing a completely different morphological structure from that of the mechanical mixture.

Comparing Fig. 3d with e, one can see that the morphologies of ZSM-5 as the core of the composite are disparate in the two figures. This can be explained as follows: after the spherical ZSM-5 particles were put in the synthesis environment of SAPO-11, the different crystallization time leads to the difference in environmental variables (such as pH value, concentrations of DPA and the precursors of silicon, aluminum and phosphorus species) around the ZSM-5 particles. Some conditions around the spherical ZSM-5 particles may restrain their growth, but promote the overgrowth of the SAPO-11 phase on their surface, resulting in the morphology that the ZSM-5 phase is enveloped by the SAPO-11 phase (Fig. 3d), similar to the growth of epitaxial FAU-on-EMT zeolite [26]. Some conditions are favorable for the dissociation of the spherical aggregate into the monocrystals and thus beneficial to their growth. A faster growth rate of the monocrystals along the axes *a* and *c* than that along the axis *b* will lead to the emergence of the rhombohedral ZSM-5 phase (Fig. 4), in accordance with the growth of the ZSM-5 monocrystal in the presence of F^- [27]. Moreover, if the growth rate of the ZSM-5 phase is fast enough to surpass that of the SAPO-11 phase, the former will protrude out of the latter, as shown in Fig. 3e.

To further confirm the existence of both ZSM-5 and SAPO-11 phases in the composite, we used SEM-EDS analysis; the results are given in Table 2. Combining Fig. 3e and Table 2, one can conclude that the rhombohedral section as the core of the composite and the pseudo-spherical aggregate as the shell of the composite correspond to the ZSM-5 phase and the SAPO-11 phase, respectively, because their compositions in the composite are consistent with those of the corresponding single phases.

3.3. FT-IR

The FT-IR spectra of the ZSM-5/SAPO-11 composite and the mechanical mixture with the same composition are shown in Fig. 5. In the mechanical mixture, the peaks at 1104, 709 and 469 cm^{-1} can be assigned to the asymmetric stretching

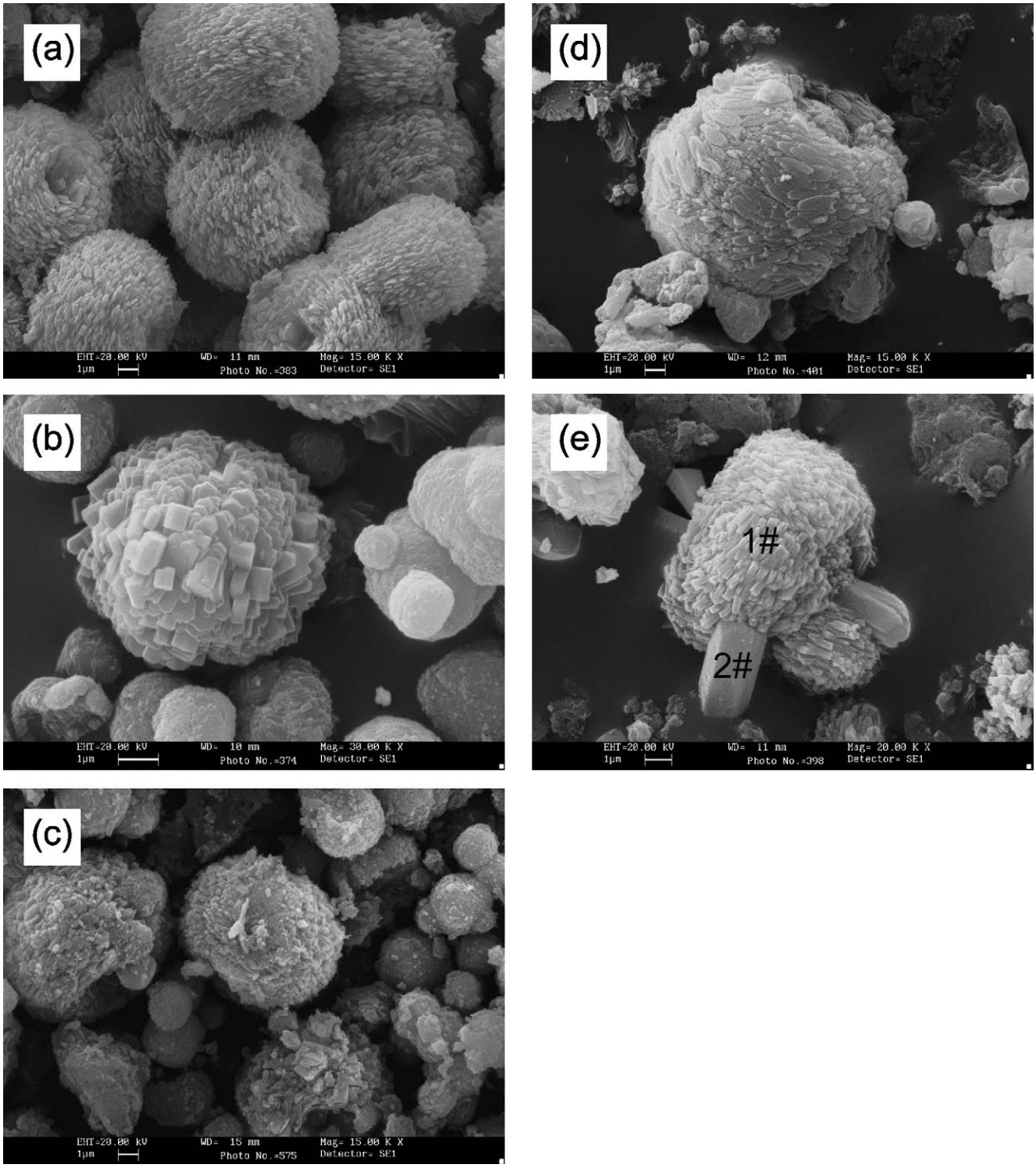

Fig. 3. SEM images of the as-synthesized samples (a) SAPO-11, (b) ZSM-5, (c) mechanical mixture, (d) composite crystallized for 24 h, and (e) composite crystallized for 42 h.

vibration, symmetric stretching vibration and bending vibration of inner tetrahedra, respectively [28]. The peak at 544 cm^{-1} can be ascribed to the asymmetric stretching vibration of five-membered rings in ZSM-5 [29] and the deformation vibration of six-membered rings in SAPO-11 [30]. Fig. 5 shows that the wavenumbers of the above peaks originally at 709, 544 and 469 cm^{-1} for the mechanical mixture now shift to 713, 548 and 472 cm^{-1} for the composite, respectively, due to the interfacial interactions between the two phases in the composite, as reported by Karlsson et al. [31] for a MFI/MCM-41 system. Meanwhile, one should also notice that the peak at 626 cm^{-1} in the mechanical mixture, standing for the deformation vibration of tetrahedron outer links of four-membered rings in SAPO-11, disappears in the composite. Because the vibration of

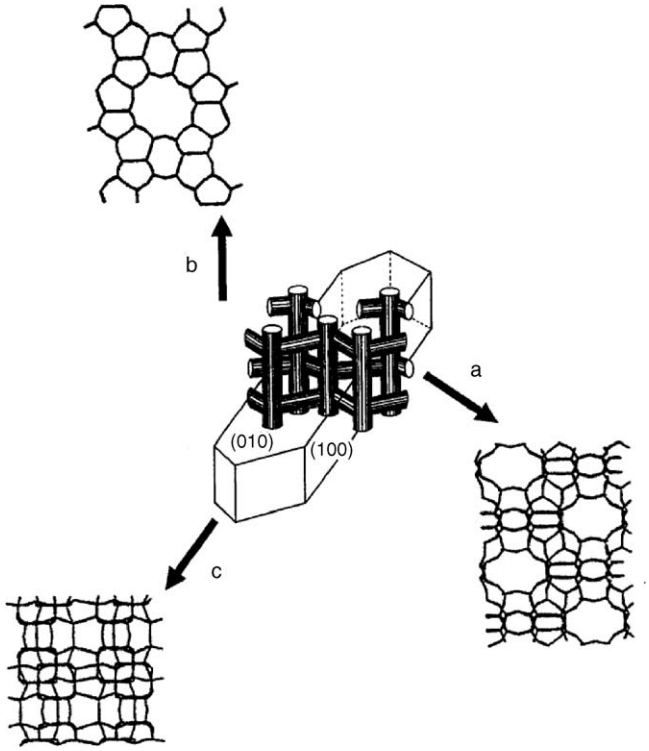

Fig. 4. General sketch of monocrystal and pore structure of ZSM-5.

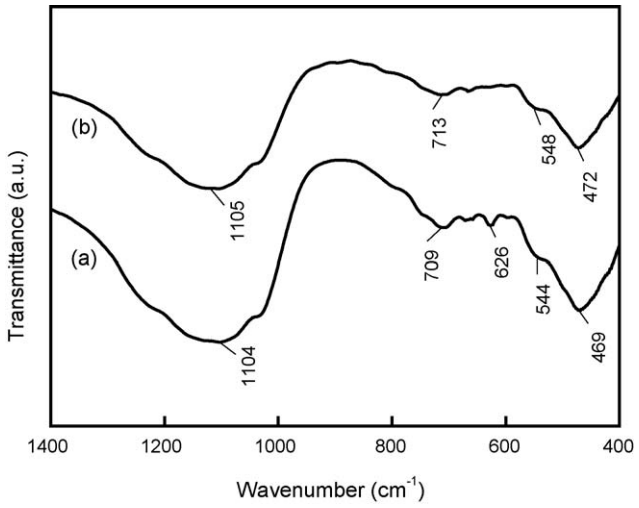

Fig. 5. IR spectra of (a) the mechanical mixture and (b) the composite in the framework vibration region.

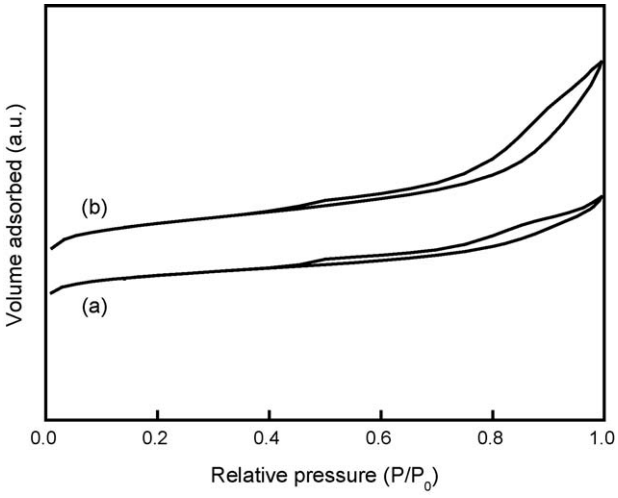

Fig. 6. N_2 adsorption–desorption isotherms of (a) the mechanical mixture and (b) the composite.

tetrahedron outer links is sensitive to any change in zeolite structure, we believe that the disappearance of the peak at 626 cm^{-1} can be attributed to a particular conjunction form of tetrahedrons and a special skeleton structure at the interface in the composite that do not exist in the mechanical mixture. The results introduced here are similar to those observed by Liu et al. [32] in synthesizing kaolin/NaY/MCM-41 composites.

3.4. Pore structure

The N_2 adsorption–desorption isotherms of the ZSM-5/SAPO-11 composite and the mechanical mixture are presented in Fig. 6. The large hysteresis loops in the two isotherms appear with the relative pressure P/P_0 ranging from 0.45 to 1.0, which can be attributed to the mesoporous structure. Obviously, the hysteresis loop of the composite is larger than that of the mechanical mixture, suggesting that, when one composites the two zeolites, more mesopores are formed due to the increscent interspaces among the different crystals.

The pore structure parameters of the samples are summarized in Table 3. Compared with SAPO-11 with a one-dimensional pore system consisting of non-intersecting elliptical 10-membered ring pores of 0.39 nm × 0.63 nm [33], ZSM-5 has more open structure owing to its two perpendicularly intersecting channel systems with the nearly circular pore openings of 0.54 nm × 0.56 nm and the elliptical pore of 0.51 nm × 0.54 nm [34]. From Table 3, it can be seen that the composite has more mesopores and fewer micropores than the mechanical mixture, so the former is superior in minimizing the side reactions by accelerating the diffusion of reactants, intermediates and products.

Table 2
Results of SEM-EDS analysis of the different samples

	SAPO-11	ZSM-5	SAPO-11 phase in composite (1#)	ZSM-5 phase in composite (2#)
SiO_2/Al_2O_3 (mol/mol)	0.43	35.8	0.54	37.6
P_2O_5/Al_2O_3 (mol/mol)	0.85	–	1.33	0.14

Table 3
Pore structure parameters of the samples

Samples	Surface area (m^2/g)			Pore volume (ml/g)		
	Micropore	Mesopore	Total	Micropore	Mesopore	Total
ZSM-5	284	82	366	0.13	0.14	0.27
SAPO-11	186	67	253	0.087	0.13	0.22
Mechanical mixture	205	70	275	0.089	0.13	0.22
Composite	178	125	303	0.082	0.25	0.33

3.5. FT-IR of adsorbed pyridine

The FT-IR spectra of adsorbed pyridine on the H-form samples in the region of 1600–1400 cm^{-1} are shown in Figs. 7–10. The bands at 1545 and 1455 cm^{-1} correspond to those specific to the pyridine molecules chemisorbed on Brönsted and Lewis acid sites, respectively [35,36], and that at 1490 cm^{-1} is ascribed to a combination of adsorbate on both Brönsted and Lewis sites.

The quantitative determination of Brönsted and Lewis acidity by FT-IR analysis is based on the integrated Lambert–Beer law:

$$A_I = C_s \varepsilon_I \quad (1)$$

where A_I (cm^{-1}) is the integrated absorbance, C_s (μmol/cm^2) is the concentration of surface acid sites, and ε_I (cm/μmol) is the integrated molar extinction coefficient.

Consequently, the concentrations of Brönsted and Lewis acid sites in reference to a unit weight of dry sample {C_{sw} (μmol/g)} can be determined by

$$C_{sw} = A_I \pi R^2 / w \varepsilon_I \quad (2)$$

where R (cm) is the radius of the sample wafer and w (g) is the weight of the dry sample.

The values of C_{sw} are determined via Eq. (2) from the values of A_I, on the basis of the spectra of the different samples shown

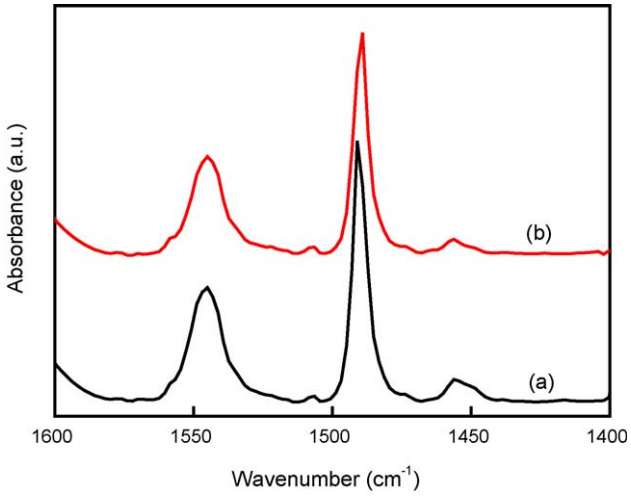

Fig. 7. IR spectra of the pyridine adsorbed on H-form ZSM-5 at (a) 473 K and (b) 623 K.

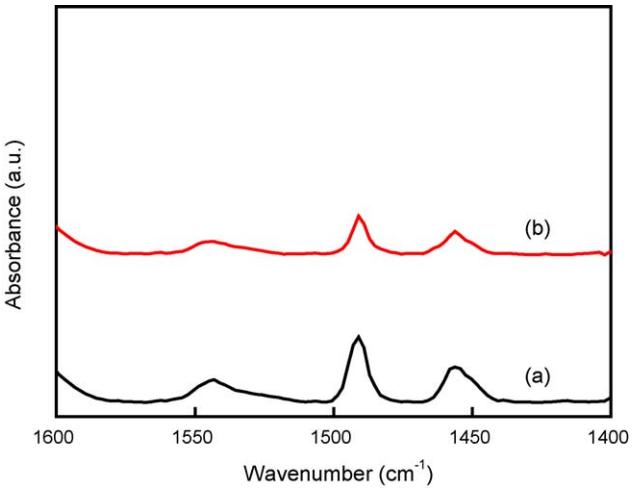

Fig. 8. IR spectra of the pyridine adsorbed on H-form SAPO-11 at (a) 473 K and (b) 623 K.

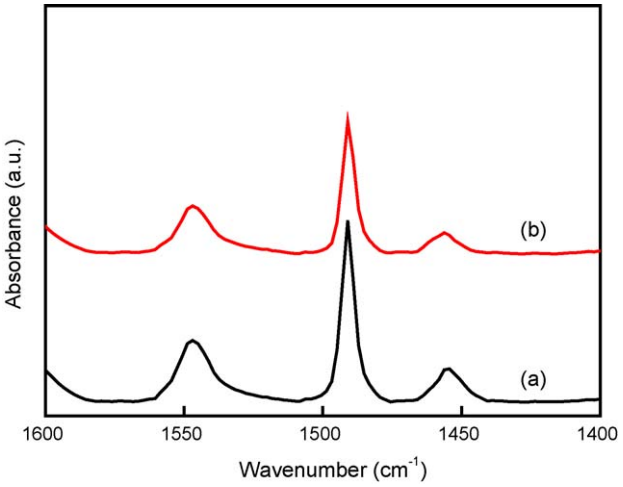

Fig. 9. IR spectra of the pyridine adsorbed on the H-form mechanical mixture at (a) 473 K and (b) 623 K.

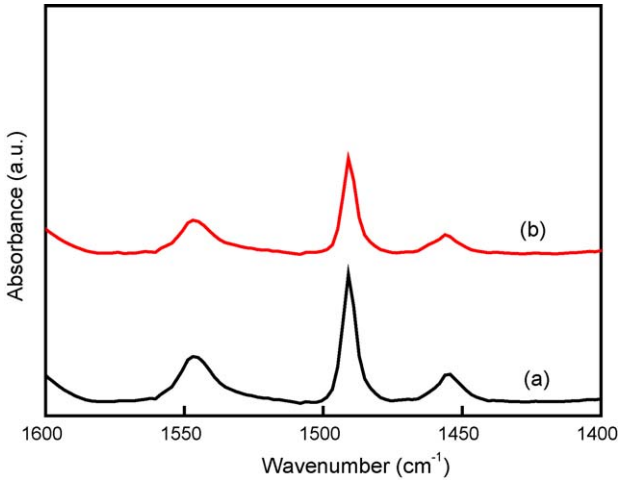

Fig. 10. IR spectra of the pyridine adsorbed on the H-form composite at (a) 473 K and (b) 623 K.

Table 4
Acidity of the samples

Samples	Acidity (μmol/g)				
	Weak acid		Medium and strong acid		Total
	Lewis	Brönsted	Lewis	Brönsted	
ZSM-5	21.4	79.7	33.3	347.5	481.9
SAPO-11	45.2	69.5	58.3	18.6	191.6
Mechanical mixture	24.3	75.4	31.6	137.1	268.4
Composite	33.8	64.7	44.6	96.1	239.2

in Figs. 7–10 and those of ε_I relative to Brönsted and Lewis acid sites calculated according to Emeis [37]. Thus, the total Brönsted and Lewis acidity can be calculated from the IR results of pyridine adsorption at 473 K, and the medium and strong Brönsted and Lewis acidity can be obtained according to the IR spectra of pyridine adsorption at 623 K.

Table 4 gives some quantitative information about the acidic properties of the H-form samples. Among the above four samples, the total acidity is in the order of ZSM-5 ≫ mechanical mixture > composite > SAPO-11; the total Lewis acidity is in the sequence of SAPO-11 > composite > mechanical mixture ≈ ZSM-5, and the total Brönsted acidity is in the order of ZSM-5 ≫ mechanical mixture > composite > SAPO-11, indicating that SAPO-11 has the most Lewis acid sites and ZSM-5 has the most Brönsted acid sites among them. As shown in Table 4, the medium and strong Brönsted acidity in ZSM-5 can be as high as up to 347.5 μmol/g, much more than the others, so the medium and strong Brönsted acidity in the mechanical mixture of ZSM-5 and SAPO-11 promptly increases from 18.6 μmol/g of SAPO-11 to 137.1 μmol/g, resulting in the great increase in the acid strength of the mechanical mixture. Compared with the mechanical mixture, the composite has moderate acid strength and an acid-type distribution that are expected to be able to enhance the synergism effect between Brönsted and Lewis acids and thus to improve the catalytic activity of the composite-derived catalyst. The appropriate acidity distribution of the composite is attributed to the conversion of some Brönsted acid sites in the ZSM-5 phase into the Lewis acid sites because of the hydrothermal effect in the subsequent synthesis of SAPO-11, as explained in the literature [38]. The acidity characteristic of the composite can be also explained as follows: as shown in Fig. 3, the ZSM-5 phase is covered in part by the SAPO-11 phase in the composite, so the surface of the composite presents an acidity distribution similar to that of the SAPO-11, which leads to the large reduction in the Brönsted acidity of the composite compared with the ZSM-5 and the mechanical mixture.

3.6. Catalytic performance

By impregnating the above four H-form samples with $(NH_4)_6Mo_7O_{24}$ and $Ni(NO_3)_2$ by the fractional step method, extruding each of them with pseudoboehmite as binder, and calcining them at 773 K for 4 h, we made the four Ni–Mo catalysts supported on ZSM-5, SAPO-11, the mechanical mixture and the composite, respectively; they are denoted as Catalyst A, B, C and D.

Table 5
Hydro-upgrading results of FCC gasoline over the four catalysts[a]

	Catalyst			
	A	B	C	D
Lumped composition of the liquid product (vol.%)				
n-Paraffins	11.3	12.3	11.5	9.2
i-Paraffins	36.3	48.7	40.2	45.3
Olefins	26.5	11.1	13.9	10.4
Naphthenes	8.3	8.7	12.0	7.5
Arenes	17.6	19.1	22.4	27.6
Benzene (vol.%)	0.45	0.51	0.53	0.47
HDS (%)	92.0	94.3	92.7	93.3
RON	86.9	87.9	89.2	91.8
Liquid yield (wt.%)	94	100	99	99
Coke (mg)	41.2	3.1	16.3	5.1

HDS: defined as the percentage conversion of total sulfur compounds in FCC gasoline. Coke: defined as the coke amount deposited on per gram catalyst.
[a] Time on stream = 24 h.

The reaction performances of the four catalysts for upgrading FCC gasoline are presented in Table 5. All the four catalysts have good HDS performance (with a HDS ratio > 90%), so the emphasis of the discussion below is placed on the hydroisomerization and aromatization activities of the catalysts.

As shown in Table 5, it is evident that, after a 24 h run, the catalyst with ZSM-5 as supporter (Catalyst A) becomes inactive in aromatization and gives the lowest *i*-paraffins content, product RON and liquid yield among the four catalysts, due to the fact that too much medium and strong Brönsted acid sites in ZSM-5 zeolite lead to the poor stability of the catalyst [15]. The catalyst with SAPO-11 as supporter (Catalyst B) shows excellent hydroisomerization activity (giving an increment of 20.4 vol.% in the *i*-paraffins content compared with that of the feedstock) and the highest liquid yield (100 wt.%) because of the weaker acid strength and the more Lewis acid sites in SAPO-11 (Table 4), but suffers a product RON loss by 3.8, fully demonstrating the inability of hydroisomerization alone in preserving gasoline RON. Compared with the two catalysts above, the catalyst with the mechanical mixture as supporter (Catalyst C) provides the product with an improved product RON, but still lower than that of the feedstock; moreover, the high coke deposition may also restrict its application. The catalyst with the ZSM-5/SAPO-11 composite as supporter (Catalyst D) displays the best aromatization activity (giving an increment of 10.2 vol.% in the arenes content compared with that in the feedstock) and HDS performance (93.3%), excellent hydroisomerization activity, and superior RON preservability, illustrating the importance of aromatization in maintaining gasoline RON. In addition to the above-mentioned advantages, Catalyst D also offers higher liquid yield and lower coke deposition, presenting itself as a potential catalyst system for further commercial development, in which the long-term stability is crucial.

The superior reaction performance of Catalyst D is closely related to the specific acidity and pore structure of the composite. As shown in the above SEM images, the ZSM-5 phase is completely separate from the SAPO-11 phase in the mechanical mixture, while the two phases in the composite are intimately bonded by the interfacial effect, and thus their synergism in acidity and pore structure is enhanced. This feature of the ZSM-5/SAPO-11 composite cannot be obtained simply by mixing the same single zeolites, as proven by Guo et al. with *n*-heptane cracking as an example reaction for a Beta/MCM-41 system [39]. Therefore, there is no doubt that the ZSM-5/SAPO-11 composite is more effective for hydro-upgrading FCC gasoline than the mechanical mixture.

4. Conclusions

ZSM-5/SAPO-11 composites were synthesized through in situ crystallization of SAPO-11 on ZSM-5 and applied to hydro-upgrading FCC gasoline. The SEM analysis results showed that the composites had the morphology with ZSM-5 as the core and SAPO-11 as the shell. Compared with the mechanical mixture consisting of individual ZSM-5 and SAPO-11, the composite had more mesopores favorable for the diffusion of substances and suitable acidity distribution advantageous to enhancing the synergism effect between Brönsted and Lewis acids. These two effects markedly improved the reaction performance of the composite-derived FCC gasoline hydro-upgrading catalyst. They thus provided a catalyst with balanced HDS, hydroisomerization and aromatization activities that contributed to RON preservation, high liquid yield and good stability in the case of the olefin and sulfur reduction. Such results mean that the ZSM-5/SAPO-11 composite-supported Ni–Mo catalyst could be taken as a potential catalyst system for hydro-upgrading FCC gasoline.

Acknowledgement

The authors acknowledge the financial support from the Ministry of Science and Technology of China through the National Basic Research Program (No. 2004CB217807).

References

[1] S. Brunet, D. Mey, G. Pérot, C. Bouchy, F. Diehl, Appl. Catal. A: Gen. 278 (2005) 143.
[2] J. Balko, D. Podratz, J. Olesen, NPRA Annual Meeting, AM-00-14, 2000.
[3] J.P. Greeley, NPRA Annual Meeting, AM-00-11, 2000.
[4] J.L. Nocca, J. Cosyns, Q. Debuisschert, B. Didillon, NPRA Annual Meeting, AM-00-61, 2000.
[5] N.P. Martinez, J.A. Salazar, G.J. Antos, M. Anand, NPRA Annual Meeting, AM-00-52, 2000.
[6] S.S. Shih, P.J. Owens, S. Palit, D.A. Tryjankowski, NPRA Annual Meeting, AM-99-30, 1999.
[7] D.D. Li, Y.L. Shi, Y.J. Hu, Y.B. Xi, M.F. Li, Y.H. Shi, CN Patent 1,465,666 (2002).
[8] Y. Fan, X.J. Bao, G. Shi, W.S. Wei, J. Xu, Appl. Catal. A: Gen. 275 (2004) 61.
[9] Y. Fan, X.J. Bao, D. Lei, G. Shi, W.S. Wei, J. Xu, Fuel 84 (2005) 435.
[10] Y. Fan, X.J. Bao, G. Shi, W.S. Wei, J. Xu, Acta Petrol. Sin. 21 (2005) 1.
[11] M. Sugioka, F. Sado, T. Kurosaka, X. Wang, Catal. Today 45 (1998) 327.
[12] D. Li, H.F. Xu, G.D. Guthrie, J. Catal. 189 (2000) 281.
[13] T. Komatsu, M. Mesuda, T. Yashima, Appl. Catal. A: Gen. 194/195 (2000) 333.
[14] V.R. Choudhary, K. Mantri, C. Sivadinarayana, Micropor. Mesopor. Mater. 37 (2000) 1.
[15] S.K. Sahoo, N. Viswanadham, N. Ray, J.K. Gupta, I.D. Singh, Appl. Catal. A: Gen. 205 (2001) 1.
[16] V. Nieminen, N. Kumar, T. Heikkilä, E. Laine, J. Villegas, T. Salmi, D.Y. Murzin, Appl. Catal. A: Gen. 259 (2004) 227.
[17] F.J. Machado, C.M. López, Y. Campos, A. Bolívar, S. Yunes, Appl. Catal. A: Gen. 226 (2002) 241.
[18] I. Eswaramoorthi, N. Lingappan, Appl. Catal. A: Gen. 245 (2003) 119.
[19] M. Höchtl, A. Jentys, H. Vinek, J. Catal. 190 (2000) 419.
[20] J. Walendziewski, B. Pniak, Appl. Catal. A: Gen. 250 (2003) 39.
[21] X.D. Huang, L.J. Wang, L.D. Kong, Q.Z. Li, Appl. Catal. A: Gen. 253 (2003) 461.
[22] P.G. Smirniotis, L. Davydov, Catal. Rev.-Sci. Eng. 41 (1999) 43.
[23] R.J. Pellet, P.K. Coughlin, A.R. Springer, R.T. Gajek, US Patent 4,861,739 (1989).
[24] C.H.M. Tsang, P.S.E. Dai, R.H. Petty, US Patent 5,888,921 (1999).
[25] B.M. Lok, C.A. Messina, R.L. Patton, R.T. Gajek, T.R. Cannan, E.M. Flanigen, US Patent 4,440,871 (1984).
[26] A.M. Goossens, B.H. Wouters, P.J. Grobet, V. Buschmann, L. Fiermans, J.A. Martens, Eur. J. Inorg. Chem. 5 (2001) 1167.
[27] W. Fan, R. Li, J. Ma, B. Fan, J. Cao, Micropor. Mater. 4 (1985) 301.
[28] P.A. Jacobs, J.A. Martens, Stud. Surf. Sci. Catal. 33 (1987) 26.
[29] O.G. Somani, A.L. Choudhari, B.S. Rao, S.P. Mirajkar, Mater. Chem. Phys. 82 (2003) 538.
[30] M. Alfonzo, J. Goldwasser, C.M. López, F.J. Machado, M. Matjushin, B. Méndez, M.M. Ramírez de Agudelo, J. Mol. Catal. A: Chem. 98 (1995) 35.
[31] A. Karlsson, M. Stöcker, R. Schmidt, Micropor. Mesopor. Mater. 27 (1999) 181.
[32] H.T. Liu, X.J. Bao, W.S. Wei, G. Shi, Micropor. Mesopor. Mater. 66 (2003) 117.
[33] J.M. Campelo, F. Lafont, J.M. Marinas, Appl. Catal. A: Gen. 152 (1997) 53.
[34] G.T. Kokotailo, S.L. Lawton, D.H. Olson, W.M. Meier, Nature 272 (1978) 437.
[35] G. Busca, Catal. Today 41 (1998) 191.
[36] J.A.Z. Pieterse, S. Veefkind-Reyes, K. Seshan, L. Domokos, J.A. Lercher, J. Catal. 187 (1999) 518.
[37] C.A. Emeis, J. Catal. 141 (1993) 347.
[38] S.M. Campbell, D.M. Bibby, J.M. Coddington, R.F. Howe, R.H. Meinhold, J. Catal. 161 (1996) 338.
[39] W.P. Guo, L.M. Huang, P. Deng, Z.Y. Xue, Q.Z. Li, Micropor. Mesopor. Mater. 44/45 (2001) 427.